Electric field effect on the intersubband optical absorption of GeSn quantum wells with parabolically graded barriers

N. Yahyaoui [a],[*], P. Baser [b], M. Said [a], S. Saadaoui [c]

[a] *Laboratoire de la Matière Condensée et des Nanosciences (LMCN), Département de Physique, Faculté des Sciences de Monastir, Avenue de l'Environnement, 5019, Monastir, Tunisia*
[b] *Department of Physics, Faculty of Science, Sivas Cumhuriyet University, Sivas, Turkey*
[c] *Department of Physics, Faculty of Science and Arts, Mohayel Aser, King Khalid University, Abha, Saudi Arabia*

ABSTRACT

In this study, we propose a theoretical simulation of a $Ge_{0.9}Sn_{0.1}$ rectangular SQW with GeSn parabolically graded barriers (PGBs) in the terahertz (THz) region. The discrete intra-band confined energy levels and their matching wave functions were calculated by solving the stationary Schrödinger equation by the finite difference method taking into account the Compact Density Matrix approach under the framework of both the effective mass and the envelope wave function approximations. In this work, we studied the effect of the quantum square-well width on the intersubband transition and oscillator strength in a GeSn-strained-based Barrier-Well-Barrier GeSn/(Ge,α-Sn) PGBs to obtain the optimum quantum confinement of electrons. The electronic states and their wave functions in the conduction band were computed by solving the Schrödinger equation without and under the effect of an applied external electric field at room temperature. We then investigated the effect of the electric field on the optical absorption coefficient (OAC). Our numerical results show that for external fields (>15 kV/cm), an intersubband transitions (ISBTs) frequency band of 2–14 THz (8–58 meV) was obtained for the specific optimized parameters. These results should be beneficial to the design of devices based on GeSn QWs with PGB structures operating in the THz frequency range.

1. Introduction

In recent years, Terahertz technology, which is located in the frequency range (0.1–10 THz) for wireless communication, which is located between the photonic and electronic ranges of the electromagnetic spectrum, has been the focus of attention for research [1]. This new technology has many applications due to its wide band gap in the THz range, such as quantum well-infrared photodetectors (QWIPs), resonant tunneling diodes (RTDs), vertical cavity surface emitting laser (VCSEL), unidirectional carrier (UTC) photodiodes, such as quantum stepped lasers, laser spectrometers and detectors [2–6]. From these structures, particularly in quantum well-infrared photodetectors (QWIPs) and quantum stepped lasers (QCLs), absorption and emission are usually due to subband interband transitions (ISBT) within the conduction band [7]. With the advancement of crystal growth techniques, it became possible to obtain devices based on ISPT and ISBT was demonstrated for the first time for the AlGaAs/GaAs semiconductor quantum well (QW) structure [8]. The frequency of AlGaAs/GaAs ISBT based systems can be varied in the mid-infrared (mid-IR) to THz spectral range. However, achieving

optical transitions at wavelengths below <3 μm in the AlGaAs/GaAs system is difficult due to the band gap and material transparency [9,10].

Two-dimensional semiconductor materials, in which the carrier movement is limited to one dimension, are in the suitable material group for THz modulators due to their properties such as adjustable band gap, doping and adjustable temperature and conductivity [11]. While thermal detectors are not preferred for many applications that require a high-speed operation, THz photon detectors obtained by using subband transitions in semiconductor quantum structures are preferred due to their advantages such as very fast response, high power, small size and adjustable frequency [12]. GaAs/AlGaAs infrared photodetector (QWIP) is one of the first examples of quantum well semiconductor structures operating in the THz region [13]. Because of all these technological applications, in this study, we focus on GeSn parabolic quantum well structure working with intersubband transitions. On the other hand, the authors in Ref. [14] have studied the effect of the free carrier densities in each subband in asymmetric stepped quantum wells. The obtained results show that the weak band offsets changes have a very slight effect on the energy levels' position and even less on their energy separation. Meanwhile, M.K. Bahar et al. [15] have investigated the influence of the free carrier densities on the linear and nonlinear optical properties of quantum dots immersed in plasma, they showed that, in each case, the increase of carrier density (σ_ν) does not affect the resonant frequencies of photons, but it leads to increase the total refractive index changes (TRICs) and total absorption coefficient TACs amplitudes due to the increment of the number of density of states. Ge from group IV semiconductors is widely used in electronic devices, but its application area is limited due to its indirect band gap structure. However, due to the low band gap of 0.14 eV, the band gap can be indirectly converted through strain or alloying with other elements of group IV by progressive band engineering techniques [16,17]. Ge lasers have been obtained with this technique. Moreover, by alloying Ge with semi-metallic α-Sn, materials with forbidden band gaps can be obtained directly from Group IV semiconductors [18]. Many studies have been done on GeSn alloys and new devices obtained from these alloys [19–22]. First demonstration of direct bandgap GeSn lasers. In this study, a direct bandgap laser obtained from group IV elements formed by alloying Ge with Sn without strain was obtained. It was found that a positive material gain can be obtained for GeSn QWs grown on Ge. For the GeSn quantum well, the Sn alloy was 15 % and the width was 12 nm [23]. In addition, $Ge_{1-x}Sn_x$ strained structures are excellent candidates for many optoelectronic applications such as lasers [24–27], light-emitting diodes [28,29], photo-detectors [30–33] and optical modulators [34].

Many optoelectronic devices use rectangular quantum wells (QWs) in their designs. Also, asymmetric QWs [35,36] and parabolic QWs (PQWs) [37,38] could be obtained by developing crystal growth techniques. Also, asymmetric quantum wells could be obtained by applying an electric field to the structure [39]. Parabolic quantum wells are an example of an asymmetric system. Quantum wells with parabolic confinement potentials allow the realization of semiconductor heterostructures that mimic the physical properties of a quantum harmonic oscillator [40]. R.C. Miller et al. proved that from photoluminescence measurements at 5 K of GaAs-A1$_{0.3}$Ga$_{0.7}$As parabolic quantum wells obtained by molecular beam epitaxy, harmonic oscillator-like electron and hole levels are formed [41].

Therefore, in recent years, PQWs have been the subject of numerous theoretical and experimental studies and have aroused considerable interest, making them well adapted to this application [42–45].

Experiments performed on group III-V materials have demonstrated that the THz intersubband could benefit from a quantum well with parabolic confinement potential [46]. Until three years later, experimental work has resulted in the development of Ge/SiGe parabolic quantum well structures with high Ge concentrations [47]. This result paves the way for the development of intersubband detectors. In 2021, Montanari et al. [48] studied THz intersubband transitions in Ge/SiGe Parabolic Quantum Wells and demonstrated that these heterostructures are promising in THz optoelectronic devices. It is interesting to note that the incorporation of Sn in the quantum well (QW) opens the possibility to achieve longer wavelength absorption compared with pure Ge [49].

Linear optical properties such as absorption and luminescence have long been used as an important factor in understanding the fundamental physics of semiconductor materials. In addition, the changes in these properties depending on the electric field were also investigated. Because the electric field changes the symmetry of the structure, it is an external parameter that can be used to adjust the electrical and optical properties. There have been many studies investigating these effects [50–54]. U. Yesilgul et al. calculated the linear and third-order nonlinear optical absorption coefficients of asymmetric double quantum well GaAs/GaAlAs under an intense laser field and the electric and magnetic field-dependent variation of the refractive index. They showed that as the intense laser field, electric field, and magnetic field values change, nonlinear optical absorption spectra and total refractive index peaks can be redshifted or blued [51]. N. D. Hien studied the linear and nonlinear optical properties of GaAs-AlGaAs semi-parabolic quantum wells (SPQW). From the results obtained, it was seen that the first three electronic energy levels vary considerably depending on the electric field, and the wave functions shift to the right as the electric field increases. It has also been proven that both linear and nonlinear optical properties are very sensitive to electric field [52].

Much work has been done calculating the oscillator strengths in QWs [54–56]. D. Bejan et al. theoretically studied the 3D structure of combined GaAs/Al$_{0.3}$Ga$_{0.7}$As triple concentric quantum rings under an electric field and intense laser field. The electric field and the laser field have opposite effects on energy levels. That is, increasing the electric field decreased energy levels while increasing ILF was found to increase energy levels. It has been proven that oscillator powers and absorption spectra can be controlled very well by external fields [55]. The energy spectrum of the system consisting of a CdS/SiO$_2$ spherical quantum dot and an electron at the ZnS/Cd$_x$Zn$_{1-x}$ S anti-dot and a donor impurity was investigated. In addition, the oscillator power of the subband transitions was calculated as the radius changed. It was observed that as the size of the quantum dot increased, the oscillator force approached the bulk semiconductor values [56]. With this motivation, we propose to simulate a semiconductor germanium-tin alloy for the design of terahertz interband transitions in which the Ge active site is replaced by a GeSn QWs.

In this study, based on our previous results regarding electronic band parameters for stretched GeSn [57], optical properties of ISBTs under electric field in a GeSn/(Ge,α-Sn) single QWs structure with parabolic grade barriers (PGBs) at RT. The first three energy levels and the probability of finding particles at these levels were determined.

In addition to these findings, the subband interband optical absorption coefficient (OAC) at room temperature and the Stark effect of the electric field on the OAC are presented and discussed.

2. Theoretical computation

A $Ge_{0.9}Sn_{0.1}$ SQW inserted between GeSn PGBs with a Sn content of 5 % at the top to 0 % below the barriers is shown in Fig. 1. The computation of the intersubband absorption coefficient (IAC) in the conduction band for GeSn QWs with GeSn PGBs was carried out by solving the Schrödinger equation. Under the effective mass approximation, the energy levels E and the corresponding wave functions in SQW can be obtained by solving Schrodinger. The time-independent Schrödinger equation in the one-dimensional case as [58]:

$$\left(-\frac{\hbar^2}{2m^*}\frac{d}{dz^2} + V(z) + qFz \right)\Psi(z) = E\,\Psi(z) \tag{1}$$

where $\Psi(z)$ is the wave functions of the electron, which is exactly obtained from the Schrödinger equation in z-direction, m^* is the effective mass of the electron, V(z) is the confinement potential profile for the electron and F is the external electric field in the z-direction. The functional form of the confinement potential is given by:

$$V(z) = \begin{cases} \left(\frac{2z}{L_{PQW}}\right)^2 V_0 \; ; \; |z| > \frac{L_{QW}}{2} \\ V_0 \; ; \quad |z| \le \frac{L_{QW}}{2} \end{cases} \tag{2}$$

where L_{QW} is the width of the central rectangular GeSn QW layer and L_{PQW} is the PQW width. For QWs, the conduction band offset (ΔE_c) is defined [57].

$$\Delta E_c = (x - y)[1.243 + (-1.816 + 0.641x)(1 + 0.167(y + x))] \tag{3}$$

An exact analytical solution of the Schrödinger equation (Eq. (1)) is clearly not possible. The eigenfunctions of the infinite potential well with the L width are taken base for solving the Schrödinger equation in the z-direction. L is well width of the infinite well at the far end of the QW with L_w well width ($L > L_w$) and its value is determined according to the convergence of the energy eigenvalues. These bases are formed as:

$$\Psi_n(z) = \sqrt{\frac{2}{L}}\cos\left(\frac{n\pi}{L}z - \delta_n\right) \tag{4}$$

where $\delta_n = \begin{cases} 0 & \text{if } n \text{ is odd} \\ \frac{\pi}{2} & \text{if } n \text{ is even} \end{cases}$

and solutions in the z-direction are described by:

$$\Psi(z) = \sum_{i=1}^{\infty} c_n \Psi_n(z) \tag{5}$$

in calculating the wavefunction $\Psi(z)$, we ensured that the eigenvalues are independent of the chosen infinite potential well width L and
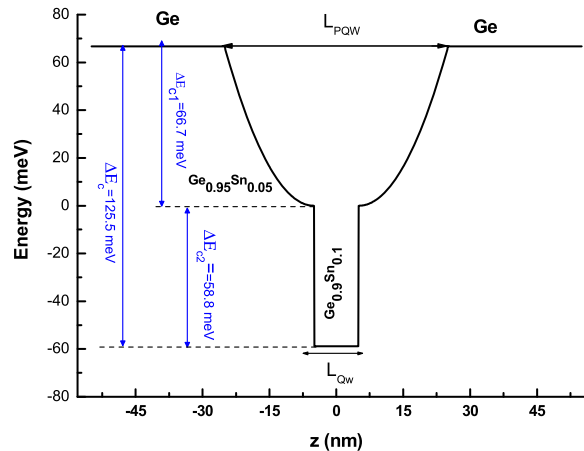

Fig. 1. Schematic diagram of GeSn QWs with PGBs.

that the wave functions are localized in the well region.

From the solution of Eq. (1), the confinement potential profile, intersubband energies, and their corresponding wave functions are obtained. After that, the intersubband OAC in GeSn/Ge PGBs can be called taken from references, and calculated according to the following expression [59,60]:

$$\alpha(\omega) = \frac{\pi e^2}{n_r c \varepsilon_0 m_0^2 \omega L_w} \sum_{i,f} |M_{if}|^2 (f_i - f_f) \left(\hbar/2\tau \Big/ \left[(E_f - E_i - \omega)^2 + \left(\hbar/\tau \right)^2 \right] \right) \tag{6}$$

where e is the electron charge, ε_0 is the free-space dielectric constant, n_r is the refractive index, L_w is the thickness of the QW, ω is the photon frequency, $E_f - E_i$ is the initial (final) state energy, M_{if} is the dipole transition matrix element between two states i and f, and f_i and f_f are the Fermi–Dirac distributions for electrons in the respective subbands. The final expression of the optical absorption co-efficient depends on the electromagnetic polarization ζ_z within the growth direction allows such transitions and the free carrier densities n_s which is taken $n_s = 4.10^{12}$ cm^{-2} [14].

3. Results and discussions

Quantum confinement energies, intersubband transitions (ISBTs), and oscillator strength are modified by the structural parameters, which are key tools for simulating the optoelectronic properties of such devices. To reach the terahertz domain, the structure based on GeSn must be optimized by changing the thicknesses of the active layers. The material parameters of Ge and α-Sn used in our simulation are obtained from Refs. [49,61,62]. The physical constants values used in this work are: $\Delta E_{c1}(Ge_{0.9}Sn_{0.1}/Ge_{0.95}Sn_{0.05}) = 58.8$ meV and $\Delta E_{c2}(Ge_{0.95}Sn_{0.05}/Ge) = 66.7$ meV. The effective mass of the materials are done: $m_c^*(Ge) = 0.038\ m_0$, $m_c^*(Sn) = 0.038 m_0$, $m_c^*(Ge_{0.95}Sn_{0.05}) = 0.0316\ m_0$, $m_c^*(Ge_{0.9}Sn_{0.1}) = 0.0295\ m_0$ and the relaxation time is taken 0.12 ps.

In Fig. 2, we illustrated the subband energies as a function of the $Ge_{0.9}Sn_{0.1}$ well width L_{Qw} with a fixed value of $L_{SPQW} = 20$ nm. This figure shows that the energy levels decrease when the layer width is larger. In this case, our computations prove that the subbands are inversely proportional to the QWs width of the QWs. Accordingly, well thickness has a significant impact on the subband energy separation in the same structure.

The energy separation between the electronic states is plotted in Fig. 3 for different values of L_{QW}, ranging from 3 to 10 nm. It is clear that the ISBTs for T_{1-2} change significantly with increasing L_{Qw}, while it changes slightly for the T_{2-3}. This was due to the quantum confinement effect. In Fig. 3, we have depicted the variation of T_{2-3} as a function of the QW width with a fixed value of the barrier width. From this figure, it can be seen that the variation of T_{2-3} changes nonlinearly with increasing well width and reaches a minimum value is around 7 nm. When the L_{QW} was less than 7 nm, the ISBT was enhanced by reducing well width. In contrast, when the L_{QW} is greater than 7 nm, T_{2-3} increased with increasing $Ge_{0.9}Sn_{0.1}$ well width. This is interpreted as the effect of the central rectangular GeSn potential on the parabolic shape of the barriers.

In addition, intersubband transitions with a frequency band from 5 to 12 THz can be obtained using specifically designed parameters. These frequency bands provide ample opportunities for applications based on these structures in the THz region.

Next, we investigated the effect of the central well width of the proposed structure on the oscillator strength using the following equation:

$$f_{i \to f} = \frac{2m_0}{\hbar^2} \left(E_i - E_f \right) \left| \langle \Psi_i | z | \Psi_f \rangle \right|^2 \tag{7}$$

where m_0 is the free electron mass, $\hbar$ is the Planck constant, $(E_i - E_f)$ is the energy difference between the two states, and $\langle \Psi_i | z | \Psi_f \rangle$ is the
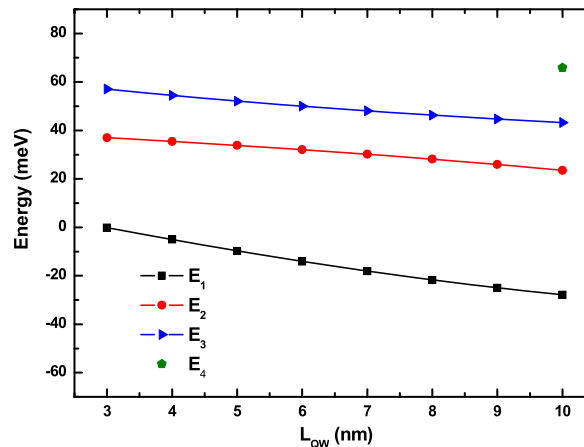

Fig. 2. The dependence of the energy levels on the QWs width with a fixed value of $L_{SPQW} = 20$ nm at RT.
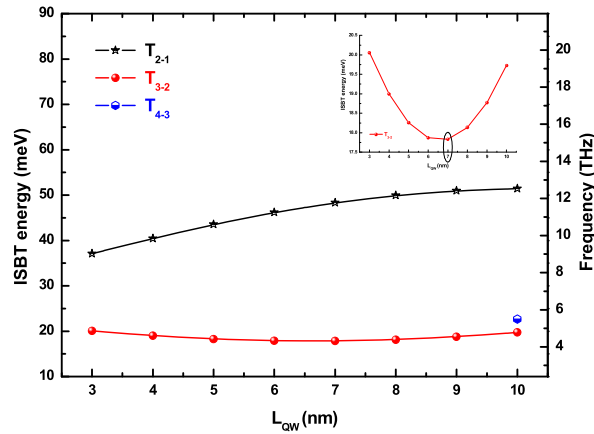
Fig. 3. The variation of ISB transition as a function of QWs width with a fixed value of $L_{SPQW} = 20$ nm at RT.

dipole matrix element.

Fig. 4 shows the variation in oscillator strengths of ISBTs versus L_{QW}. It is well known that the energy difference affects oscillator strengths. As a result, it is similar to Fig. 3 in that the oscillator strength of T_{1-2} increases dramatically, whereas the oscillator strength of T_{2-3} first decreases and then increases with the increasing width of the quantum well. The minimum oscillator strength for T_{2-3} was achieved for a well width of 7 nm, as shown in the inset of Fig. 4. Interestingly, the oscillator strength and ISBTs of T_{2-3} all reach their extremes at $L_{QW} = 7$ nm. Therefore, we can conclude that the optimal square well width of the ISB THz transition in GeSn PGBs should not be less than 7 nm. In this context, we concluded that the electronic properties are tuning by the well width. Our numerical results are in good agreement with those of reference [63].

Using the above results, we modeled the intersubband absorption coefficient in the conduction band of the considered structure based on GeSn alloys, with and without the effect of an external electric field. The modeled structure consists of $Ge_{0.9}Sn_{0.1}$ sandwiched between $Ge_{0.95}Sn_{0.05}$ barriers. Here, the structure is assumed to develop on the relaxed Ge.

We simulated the conduction band of the considered structure based on the GeSn alloys. The modeled structure consisted of $Ge_{0.9}Sn_{0.1}$ sandwiched by $Ge_{0.95}Sn_{0.05}$ barriers. The structure here is assumed to be grown on relaxed Ge. The results are studied under the condition of $L_{Qw} = 8$ nm and the composition of the GeSn alloy was taken at 10 %.

The simulation results of 8 nm width and 10 % Sn content in GeSn SQW with GeSn PCBs from 5 % Sn in the claddings to Ge are shown in Fig. 5. These compositions and thicknesses are chosen such that they form graded barriers with SQW at the center, which could provide favorable carrier confinement of electrons for the proposed stack.

For a better understanding of the optical properties, we calculated the intersubband absorption coefficient as a function of the photon energy and their corresponding frequencies for the proposed model at RT. The results are illustrated in Fig. 6 without taking into account the effect of the electric field F. From this figure, we see that the appearance of two resonance peaks is associated with the T_{1-2} transition of the deep well and the other is associated with the T_{2-3} transition of the shallow well and that only the intersubband transitions with the change of parity are authorized in a PGB GeSn QWs, as illustrated in the inset block diagram. Resonance peaks appeared at 50 meV for T_{1-2} and 18 meV for T_{2-3}. This corresponds to approximately 12 and 4 THz, respectively, with F = 0 kV/cm.
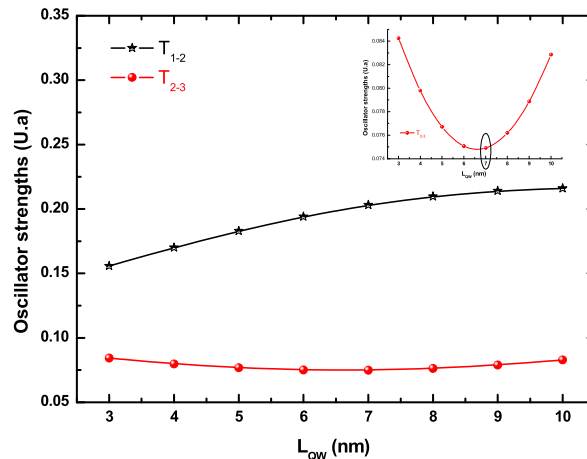

Fig. 4. The variation of the oscillator strength as a function of QWs width with a fixed value of $L_{SPQW} = 20$ nm at RT.
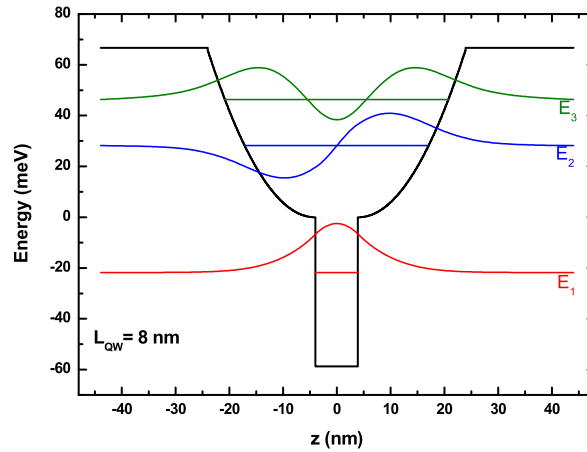
Fig. 5. The potential profile, the energy levels, and their corresponding wave functions in GeSn/Ge parabolic QWs.
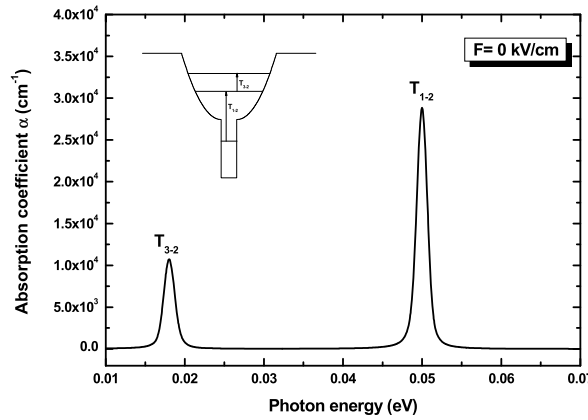

Fig. 6. The variation of optical ACs associated with T_{1-2} and T_{3-2} transitions as a function of photon energy at RT.

To cover the terahertz frequency domain in GeSn/Ge PGBs, we have investigated the influence of an applied electric field on the ISBTs energies as well as the intersubband absorption coefficient. In Fig. 7, we have depicted T_{1-2}, T_{2-3} and T_{3-4} ISBTs energies, and their corresponding frequencies as a function of the applied electric field at RT. From this figure, it can be seen that when the electric field increases, the intersubband transition T_{1-2} shifts to lower frequencies, whereas the T_{2-3} moves to larger frequencies. This shift was due to the effect of an external electric field on the PQW structure. We also note that the transitions occur at lower frequencies (<10 THz) when F > 15 kV/cm.

The variation in IOAC associated with ISBTs for the same structure at room temperature is illustrated in Fig. 8, with a fixed value of F at 17 kV/cm. From this figure, it can be seen that the transition energies T_{1-2} and T_{2-3} coincide and the magnitude of optical absorption presents a significant increase at the corresponding energies, at 9 THz. The same behavior was observed by A. Smayh et al. [14] when they investigated the optical absorption coefficient in an asymmetric stepped quantum well GaAs/Al$_y$Ga$_{1-y}$As/Al$_x$Ga$_{1-x}$As in the terahertz range, This may be useful in devices using two-photon absorption at frequencies within the terahertz domain, based on an asymmetric quantum well, and the other at 4 THz for T_{3-4} for F = 17 kV/cm. Consequently, the external electric fields led to an increase in the amplitude of the resonance peaks and played an important role in shifting the absorption spectra. Our simulation results show that we modeled an optoelectronic device operating in the 2–14 THz frequency band without considering the polarization effect. Our results are in close agreement with those of reference [64] when the authors modeled Ga(As, Bi)/AlGaAs PQW, they showed that the effect of the variation in the width of the central well leads to the manufacture of optoelectronic devices that operate in the same frequency band. Indeed, PQW-based structures are used to design optoelectronic devices covering the frequency band from 2.5 THz to 7 THz. Thus, GeSn rectangular quantum wells with GeSn (PGBs), compared to III-V compounds, have attracted the attention of researchers in recent decades for the fabrication of multicolor THz detectors.

4. Conclusions

To our knowledge, the study of THz intersubband transitions in GeSn material systems with different shapes of potential has not yet
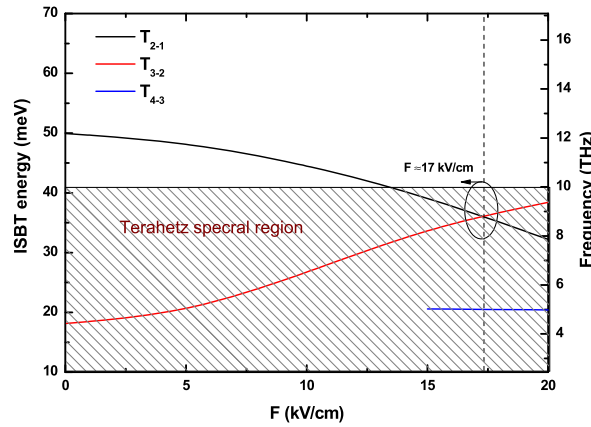
Fig. 7. The variation of ISB transition as a function of the external electric field F for fixed values L_{QW} = 8 nm and L_{SPQW} = 20 nm at RT.
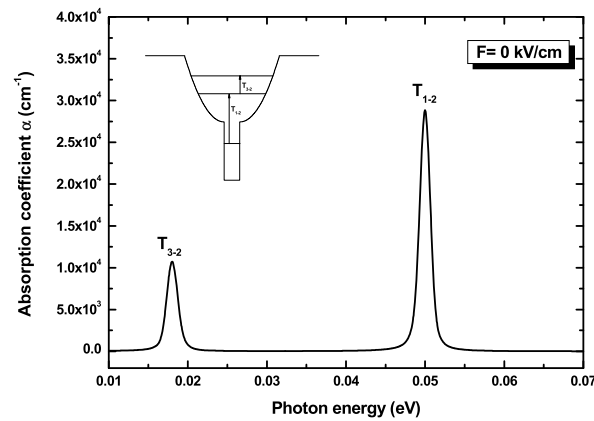

Fig. 8. The variation of optical ACs associated with T_{1-2}, T_{3-2} and T_{4-3} transitions as a function of photon energy under condition F = 17 kV/cm for fixed values of L_{QW} = 8 nm and L_{SPQW} = 20 nm at RT.

been investigated. In conclusion, we have theoretically studied the IOCA of SQWs with parabolically graded barriers (PGBs) based on group IV semiconductors. Our computations were based on the solution of the Schrödinger equation with and without an applied electric field by varying the GeSn SQW width. For an optimal square well width of 8 nm, the ISB transition energies and IOAC dependence of the applied electric field were investigated at RT in this study. The simulation results show that the IOAC is in the frequency band of 4–10 THz when an external electric field F > 15 kV/cm is applied. PGB structures with strained GeSn show great potential in photonic devices and optoelectronics and achieve high performance for the optimization of THz detectors.

Author agreement statement

We the undersigned declare that this manuscript is original, has not been published before and is not currently being considered for publication elsewhere. We confirm that the manuscript has been read and approved by all named authors and that there are no other persons who satisfied the criteria for authorship but are not listed. We further confirm that the order of authors listed in the manuscript has been approved by all of us. We understand that the Corresponding Author is the sole contact for the Editorial process. He/she is responsible for communicating with the other authors about progress, submissions of revisions and final approval of proofs Signed by all authors as follows.

Declaration of competing interest

This manuscript has not been submitted to, nor is under review at, another journal or other publishing venue.

Data availability

No data was used for the research described in the article.

Acknowledgements

References

[1] G. Carpintero, E. García-Muñoz, H. Hartnagel, S. Preu, A. Raisanen (Eds.), Semiconductor TeraHertz Technology: Devices and Systems at Room Temperature Operation, John Wiley & Sons, Chichester, UK, 2015.
[2] J.-S. Rieh, Introduction to Terahertz Electronics, Springer, Cham, Switzerland, 2020.
[3] Y.S. Lee, Principles of Terahertz Science and Technology, Springer, Boston, USA, 2009.
[4] W. Salhi, A. Samyh, A. Rajira, H. Akabli, A. Almaggoussi, A. Abounadi, Phys. B Condens. Matter 639 (2022), 413955.
[5] E. Dupont, P.B. Corkum, H.C. Liu, P.H. Wilson, M. Buchanan, Z.R. Wasilewski, Appl. Phys. Lett. 65 (1994) 1560.
[6] H. Kaur, M. Singh, A. Chauhan, R. Sharma, Mater. Today Proc. 26 (2020) 3458.
[7] Y. Wang, M. Haraguchi, X. Zhang, P. Wang, S. Sun, Coatings 13 (2023) 972.
[8] L.C. West, S.J. Eglash, Appl. Phys. Lett. 46 (1985) 1156.
[9] B. Gil, III-nitride Semiconductors and Their Modern Devices, Oxford University Press, Oxford, 2013.
[10] D.H. Mudiyanselage, D. Wang, Y. Zhao, H. Fu, J. Appl. Phys. 131 (2022), 210901.
[11] T. Kleine-Ostmann, P. Dawson, K. Pierz, G. Hein, M. Koch, Appl. Phys. Lett. 84 (2004) 3555.
[12] H. Luo, H.C. Liu, C.Y. Song, Z.R. Wasilewski, Appl. Phys. Lett. 86 (2005) 231103 (1)–231103 (3).
[13] H. Schneider, H. C. Liu, Quantum Well Infrared Photodetectors Physics and Applications, Springer Series in optical sciences..
[14] A. Samyh, W. Salhi, A. Rajira, H. Akabli, A. Abounadi, A. Almaggoussi, Superlattice. Microst. 130 (2019) 560–568.
[15] M.K. Bahara, F. Unganb, A. Soylu, Phys. E Low-dimens. Syst. Nanostruct. 114 (2019), 113567.
[16] J. Liu, et al., Opt Express 15 (2007) 11272–11277.
[17] X. Sun, J. Liu, L. Kimerling, J. Michel, IEEE J. Sel. Top. Quant. Electron. 16 (2010) 124–131.
[18] S. Zaima, et al., Sci. Technol. Adv. Mater. 16 (2015), 043502.
[19] R.A. Soref, C.H. Perry, J. Appl. Phys. 69 (1991) 539–541.
[20] G. He, H. Atwater, Phys. Rev. Lett. 79 (1997) 1937–1940.
[21] J. Xie, et al., Chem. Mater. 22 (2010) 3779–3789.
[22] H. Lin, R. Chen, Y.J. Huo, T.I. Kamins, J.S. Harris, Thin Solid Films 520 (2012) 3927–3930.
[23] S. Wirths, et al., Nat. Photonics 9 (2015) 88–92.
[24] G.E. Chang, S.W. Chang, S.L. Chuang, IEEE J. Quant. Electron. 46 (2010) 1813–1820.
[25] D. Stange, N. von den Driesch, T. Zabel, F. Armand-Pilon, D. Rainko, B. Marzban, P. Zaumseil, J.-M. Hartmann, Z. Ikonic, G. Capellini, S. Mantl, H. Sigg, J. Witzens, D. Grützmacher, D. Buca, ACS Photonics 5 (2018) 4628–4636.
[26] Y. Zhou, W. Dou, W. Du, S. Ojo, H. Tran, S.A. Ghetmiri, J. Liu, G. Sun, R. Soref, J. Margetis, J. Tolle, B. Li, Z. Chen, M. Mortazavi, S.-Q. Yu, ACS Photonics 6 (2019) 1434–1441.
[27] S. Assali, J. Nicolas, S. Mukherjee, A. Dijkstra, O. Moutanabbir, Appl. Phys. Lett. 112 (2018), 251903.
[28] T. Pham, W. Du, H. Tran, J. Margetis, J. Tolle, G. Sun, R.A. Soref, H.A. Naseem, B. Li, S.-Q. Yu, Opt Express 24 (2016) 4519.
[29] H. Tran, T. Pham, W. Du, Y. Zhang, P.C. Grant, J.M. Grant, G. Sun, R.A. Soref, J. Margetis, J. Tolle, B. Li, M. Mortazavi, S.-Q. Yu, J. Appl. Phys. 124 (2018), 013101.
[30] C. Chang, H. Li, S.H. Huang, H.H. Cheng, G. Sun, R.A. Soref, Appl. Phys. Lett. 108 (2016) 151101.
[31] H. Cong, C. Xue, J. Zheng, F. Yang, K. Yu, Z. Liu, X. Zhang, B. Cheng, Q. Wang, IEEE Photon. J. 8 (2016) 1.
[32] J. Zheng, S. Wang, Z. Liu, H. Cong, C. Xue, C. Li, Y. Zuo, B. Cheng, Q. Wang, Appl. Phys. Lett. 108 (2016), 033503.
[33] J. Werner, M. Oehme, M. Schmid, M. Kaschel, A. Schirmer, E. Kasper, J. Schulze, Appl. Phys. Lett. 98 (2011), 061108.
[34] P. Moontragoon, N. Vukmirovic, Z. Ikonic, P. Harrison, IEEE J. Sel. Top. Quant. Electron. 16 (2010) 100–105.
[35] J. Frigerio, V. Vakarin, P. Chaisakul, M. Ferretto M, D. Chrastina, X. Le Roux, L. Vivien, G. Isella, D. Marris-Morini, Sci. Rep. 5 (2015), 15398.
[36] J. Frigerio, A. Ballabio, M. Ortolani, M. Virgilio, Opt Express 26 (2018) 31861–31872.
[37] N.D. Hien, J. Phys. Chem. Solid. 161 (2022), 110456.
[38] S. Pūkienė, M. Karaliūnas, A. Jasinskas, E. Dudutienė, B. Čechavičius, J. Devenson, R. Butkutè, A. Udal, G. Valušis, Nanotechnology 30 (2019), 455001.
[39] M.M. Fejer, S.J.B. Yoo, R.L. Byer, A. Harwit, J.S. Harris Jr., Phys. Rev. Lett. 62 (1989), 1041.
[40] A. Ballabio, J. Frigerio, S. Firoozabadi, D. Chrastina, A. Beyer, K. Volz, G. Isella, J. Phys. Appl. Phys. 52 (2019), 415105.
[41] R.C. Miller, A.C. Gossard, D.A. Kleinman, O. Munteanu, Phys. Rev. B 29 (1984), 3740(R).
[42] L. Brey, N.F. Johnson, B.I. Halperin, Phys. Rev. B 40 (1989) 10647–10649.
[43] Y. Huang, C. Lien, J. Appl. Phys. 75 (1994) 3223–3225.
[44] K.X. Guo, S.W. Gu, Phys. Rev. B 47 (1993) 16322–16325.
[45] L. Zhang, H. Xie, J Physica E 22 (2004) 791–796.
[46] A. Tzimis, A.V. Trifonov, G. Christmann, S.I. Tsintzos, Z. Hatzopoulos, I.V. Ignatiev, A.V. Kavokin, Savvidis, Appl. Phys. Lett. 107 (2015), 101101.
[47] Andrea Ballabio, Jacopo Frigerio, Saleh Firoozabadi, Daniel Chrastina, Andreas Beyer, Kerstin Volz, Giovanni Isella, J. Phys. D Appl. Phys. 52 (2019), 415105.
[48] M. Montanari, C. Ciano, L. Persichetti, C. Corley, L. Baldassarre, M. Ortolani, L. Di Gaspare, G. Capellini, D. Stark, G. Scalari, Appl. Phys. Lett. 118 (2021), 163106.
[49] N. Yahyaoui, N. Sfina, J.-L. Lazzari, A. Bournel, M. Said, J. Appl. Phys. 115 (2014), 33109.
[50] S. Schmitt-Rink, D.S. Chemla, D.A.B. Miller, Adv. Phys. 38 (1989) 89–188.
[51] U. Yesilgul, E.B. Al, J.C. Martínez-Orozco, R.L. Restrepo, M.E. Mora-Ramos, C.A. Duque, F. Ungan, E. Kasapoglu, Opt. Mater. 58 (2016) 107–112.
[52] N.D. Hien, Micro and Nanostructures 170 (2022), 207372.
[53] Z.-H. Zhang, Y.-S. Shi, J.-H. Yuan, Commun. Theor. Phys. 74 (2022), 65502.
[54] S. Haghighi, A. Haghighatzadeh, A. Attarzadeh, The European Physical Journal Plus 138 (2023) 145(1)–145(13).
[55] D. Bejana, A. Radub, C. Stan, Philosophical, 2023.
[56] V.A. Holovatsky, O.M. Makhanets, O.M. Voitsekhivska, Phys. E Low-dimens. Syst. Nanostruct. 41 (2009) 1522–1526.
[57] N. Yahyaoui, N. Sfina, J.-L. Lazzari, A. Bournel, M. Said, Superlattice. Microst. 85 (2015) 629–637.
[58] N. Yahyaoui, N. Sfina, J.-L. Lazzari, A. Bournel, M. Said, Eur. Phys. J. B 86 (2015) 259.
[59] W. Liu, D.H. Zhang, W.J. Fan, X.Y. Hou, Z.M. Jiang, J. Appl. Phys. 104 (2008) 53119 (1)–53119 (8).
[60] M. Courel, J.C. Rimada, L. Hernández, Prog. Photovoltaics Res. Appl. 21 (2012) 276–282.
[61] W.J. Yin, X.G. Gong, S.H. Wei, Phys. Rev. B 78 (2008), 161203.
[62] S.S. Chang, S.L. Chuang, IEEE J. Quant. Electron. 43 (2007) 249.
[63] E. Kasapoglu, C.A. Duque, M.E. Mora-Ramos, R.L. Restrepo, F. Ungan, U. Yesilgul, H. Sari, I. Sokmen, Mater. Chem. Phys. 154 (2015) 170–175.
[64] M. Karaliūnas, A. Udal, G. Valušis Lithuanian, J. Phys. 60 (2020) 113–124.